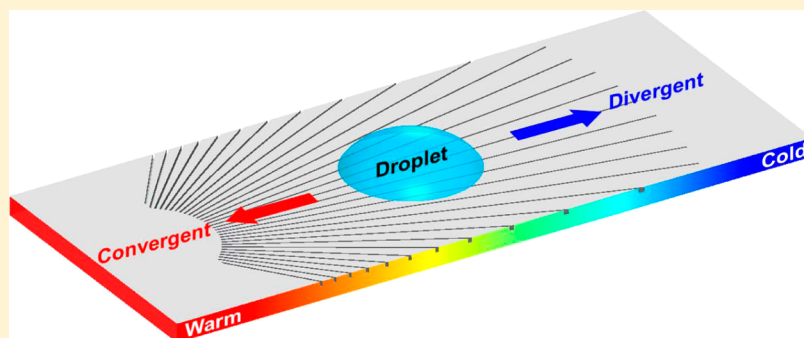


On the Thermocapillary Migration on Radially Microgrooved Surfaces

Qingwen Dai,^{*} Yajuan Ji, Wei Huang, and Xiaolei Wang

National Key Laboratory of Science and Technology on Helicopter Transmission, Nanjing University of Aeronautics & Astronautics, Nanjing 210016, China



ABSTRACT: Thermocapillary migration describes the phenomenon in which a droplet placed on a nonuniformly heated surface can migrate from warm to cold regions. Herein, we report an experimental investigation of the migration of silicone oil droplets on radially microgrooved surfaces subjected to a thermal gradient; the effects of the initial divergence angle and divergent direction on the migration behavior are highlighted. A theoretical model is established to predict the migration velocity considering the thermocapillary, viscous resistance, and radial structure-induced forces; furthermore, the proposed theoretical derivation is validated. This study advances the understanding of this interfacial phenomenon, which has great potential for regulating and controlling liquid motion in lubrication systems, condensation and heat-transfer devices, and open microfluidics.

INTRODUCTION

The spreading of droplets on a surface is a complex dynamic phenomenon that occurs at the triple-phase interface, in which the well-known Marangoni effect describes movement induced by unbalanced interfacial tension.^{1–6} A droplet placed on a nonuniformly heated hydrophilic surface can migrate from warm to cold regions in the absence of external forces.^{7–11} This motion is manifested as thermocapillary migration and has attracted significant research interest for numerous applications such as bearings, condensation devices, and microelectronics.^{12–16} Typically, rubbing surfaces encountering thermal gradients can yield starved or even dry lubrication conditions.¹⁷ In condensation assemblies, this migration can guide the flow of liquid, enhancing the condensation and heat-transfer efficiency.¹⁸ Given that thermocapillary migration occurs on solid surfaces, investigations of this phenomenon, particularly on mitigating or reinforcing it, mainly focus on the surface topography.

Over the past few decades, surfaces have been structured, textured, or engineered with micropatterns to alter the surface/interface properties.^{19–22} Regularly patterned microgrooves are one of the representative structures and have been widely investigated.²³ The study of Grützmacher et al.²⁴ and our previous study²⁵ revealed that on surfaces with a regular pattern of microgrooves, the migration parallel to the patterned microgrooves was accelerated, whereas it was pinned when

perpendicular to the pattern. This anisotropic property is appealing and has inspired researchers to design heterogeneous, mixed, or gradient patterns of microgrooves to achieve better performance.

By systematically changing the width of the grooves, Sommers et al.²⁶ achieved a variable-width microgroove pattern to control droplet motion in a direction perpendicular to the grooves. Similarly, Grützmacher et al.²⁷ designed a multiwidth mixed microgroove pattern to enhance motion parallel to the grooves. Bliznyuk et al.²⁸ fabricated stripe-patterned microgrooves with different area densities, which exhibited preferential liquid spreading in the direction parallel to the stripes. Moreover, properly designed gradient microgroove shapes, such as triangle grooves, can alter the liquid movement.²⁹

These intelligently designed microgroove patterns have exhibited many idiosyncratic capabilities for regulating liquid migration. In addition to the shape, geometry, density, and arrangement of microgroove patterns, radial gradient microgrooves represent a typical pattern configuration. Intuitively, radially designed microgrooves appear to be advantageous for guiding, gathering, and converging a liquid on the surface,

Received: May 7, 2019

Revised: June 11, 2019

Published: June 21, 2019

where the initial divergence angle between two adjacent grooves and the divergent direction are very important parameters. Confirming and enhancing these features has great potential for applications in condensation and heat-transfer devices. However, a review of the available literature indicates that there is little experimental and analytical data available regarding the migration on radially microgrooved surfaces.

Hence, in this study, thermocapillary migration experiments with silicone oil droplets were performed on silicon substrates with radial microgroove patterns. The effects of the divergent direction and initial divergence angle on the migration velocity were investigated. A theoretical model was established to predict the migration velocity considering the thermocapillary, viscous resistance, and radial structure-induced forces. The experimental and theoretical results were compared, and the proposed theoretical derivation was validated.

MATERIALS AND METHODS

Materials. The solid substrate was fabricated from a single-crystal silicon wafer with dimensions of $55 \times 25 \times 0.5$ mm, and the average surface roughness, R_a , was approximately 3 nm. Common silicone oil was employed for all of the migration tests in this study, and its major properties are presented in Table 1.

Table 1. Physical and Chemical Parameters of Silicone Oil at 40 °C

molecular formula	parameter	symbol	value
[Si(CH ₃) ₂ O] _n	dynamic viscosity	μ_0	100 mPa s
	density	ρ	0.963 g/mm ³
	viscosity–temperature coefficient	b	−0.01814 °C ^{−1}
	droplet volume	V	5 μ L

The surface tension of a liquid decreases with the increasing temperature, and this variation tendency can be described as follows

$$\gamma(T) = \gamma_0 - \gamma_T(T - T_0) \quad (1)$$

where $\gamma(T)$ and γ_0 represent the surface tension at the temperature T and reference temperature T_0 , respectively, and γ_T represents the surface-tension coefficient, $\gamma_T = \frac{\partial \gamma}{\partial T}$.

In this study, by measuring the surface tensions at different temperatures via the Wilhelmy plate method, the surface-tension coefficient was calculated, as shown in Figure 1. The contact angle is an important parameter that represents the effect of interaction between a liquid and solid. It was measured via the sessile drop

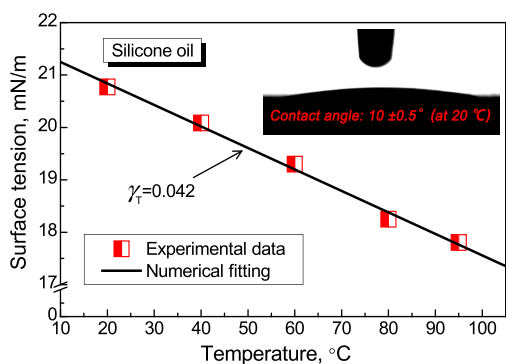


Figure 1. Correlation between the surface tension and temperature for silicone oil and the contact angle on a smooth silicon surface.

method at room temperature (approximately 20 °C). By placing a 3 μ L silicone oil droplet on a smooth silicon surface and capturing the image when the equilibrium state was reached, the contact angle was determined, which was approximately $10 \pm 0.5^\circ$.

Methods. Figure 2a shows a schematic of the migration apparatus. The basic principle was the use of temperature-controllable heating and cooling components to generate a thermal gradient on the substrate surface; detailed information regarding this apparatus is available in our previous paper.³⁰ Radial microgrooves were fabricated on the silicon substrate via photolithography combined with a wet etching process, as described in previous work.³¹ Figure 2b presents optical and micro-three-dimensional (3D) topographic images of the silicon substrate with an initial divergence angle (α) of 3° . As shown, the convergent and divergent directions are defined as the direction of a droplet moving toward and away from the initial divergent point, respectively, and the initial divergence angle is defined as the angle between two adjacent grooves. Table 2 presents the geometric parameters of the radial microgrooves, where w and d_0 represent the width and depth of each microgroove, l_0 represents the minimum distance between the individual microgrooves at the initial divergent point, and α represents the initial divergence angle.

As shown in Figure 2a, the effective length in the migration test was approximately 50 mm. The temperatures of the heating and cooling elements were set as 110 and 0 °C, respectively, generating a thermal gradient of 2.2 °C/mm on the substrate surface. By reversing the radially microgrooved substrate, experiments were performed in both the convergent and divergent directions. Silicone oil droplets with a constant volume of 5 μ L were placed at the center of the substrate, and the dynamic migration process was captured using a digital camera. By extracting key frames from the videos and using the front edge of the droplets as a reference, the migration distance and spreading area were measured. Then, the migration velocity within each second was calculated.

RESULTS AND DISCUSSION

Migration Behavior on Radially Microgrooved Surfaces. Figure 3 shows the result of a 5 μ L silicone oil droplet migrating on a radially microgrooved surface ($\alpha = 3^\circ$) in the convergent and divergent directions subject to a thermal gradient of 2.2 °C/mm. Key video frames captured during the initial 30 s were extracted, as shown in Figure 3a. Migration occurred from warm to cold regions under the effect of the thermal gradient. As the migration progressed, the droplet migrated faster in the convergent direction than in the divergent direction, whereas the surface area of the droplet on the convergent surface appeared to be smaller than that on the divergent surface.

Figure 3b shows the quantitative results for the migration velocity (scatter points), migration distance (line-symbol series), and surface area (dashed line-symbol series) of the droplets versus the elapsed time. Initially, the migration distance on the convergent surface was slightly higher than that on the divergent surface, and they both increased gradually over time. The migration velocity decreased rapidly and then gradually, and the convergent surface yielded a higher migration velocity than the divergent surface. The surface area of the droplet on the divergent surface increased significantly more than that on the convergent surface.

Figure 4 shows the influence of the divergence angle (α) on the migration performance. Migration experiments were performed in the divergent direction on substrates with divergence angles (α) of 1° and 3° under a thermal gradient of 2.2 °C/mm. Within 30 s, the droplet migrated farther on the surface with $\alpha = 1^\circ$ than that on the surface with $\alpha = 3^\circ$. The initial migration velocity on the surface with $\alpha = 1^\circ$ was

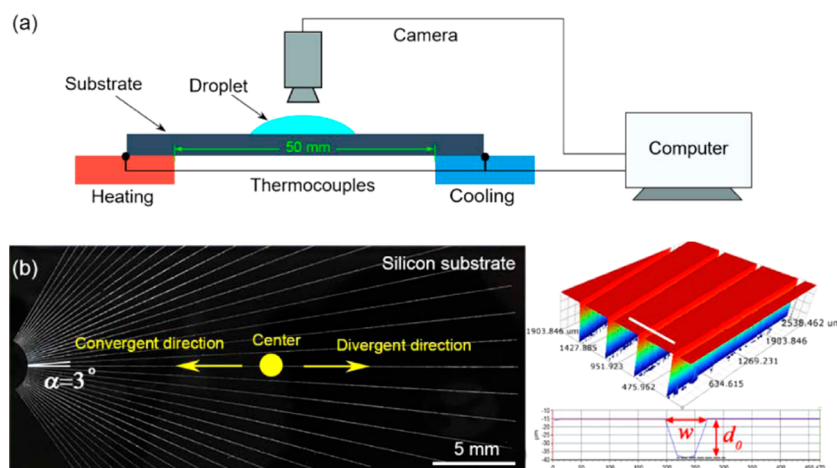


Figure 2. (a) Schematic of the migration apparatus; (b) optical and micro-3D topographic images of the silicon substrate with an initial divergence angle (α) of 3° .

Table 2. Geometric Parameters of the Radial Microgrooves

parameter	symbol	value
divergence angle	α	1°
		3°
width	w	$50 \mu\text{m}$
depth	d_0	$25 \mu\text{m}$
minimum distance	l_0	$100 \mu\text{m}$

approximately 1.5 mm/s, which was 50% higher than that (1.02 mm/s) on the surface with $\alpha = 3^\circ$.

The experimental results indicate that the geometric parameters of radially grooved surfaces have a significant effect on the migration performance, and the migration velocities on surfaces with different divergent directions and angles are significantly different. To further elucidate the influence mechanism, a theoretical analysis was described in the following section.

Theoretical Hypothesis. Theoretical models of a droplet migrating on an ideal smooth surface can be established by balancing the thermal gradient-induced driving force with the viscous resistance force.^{32,33} When a regular microgroove pattern is applied to a surface, the groove capillary effect

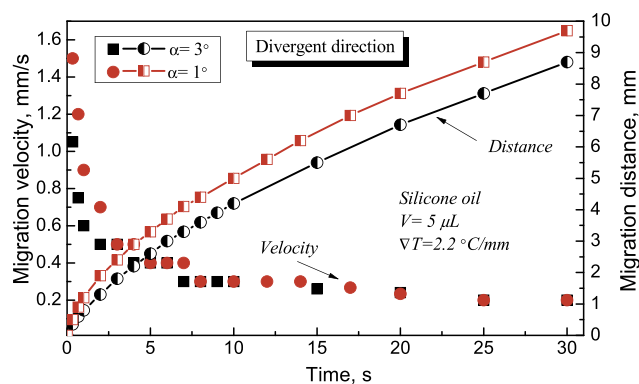


Figure 4. Influence of the divergence angle (α) on the droplet migration behavior under a thermal gradient of $2.2^\circ\text{C}/\text{mm}$.

should be considered. Because the contact angle of silicone oil on the silicon surface is only approximately 10° , according to Brochard³² and our previous study,³⁴ it is reasonable to regard the droplet as a thin film with curved edges. Therefore, the thin-film lubrication approximation theory can be employed to

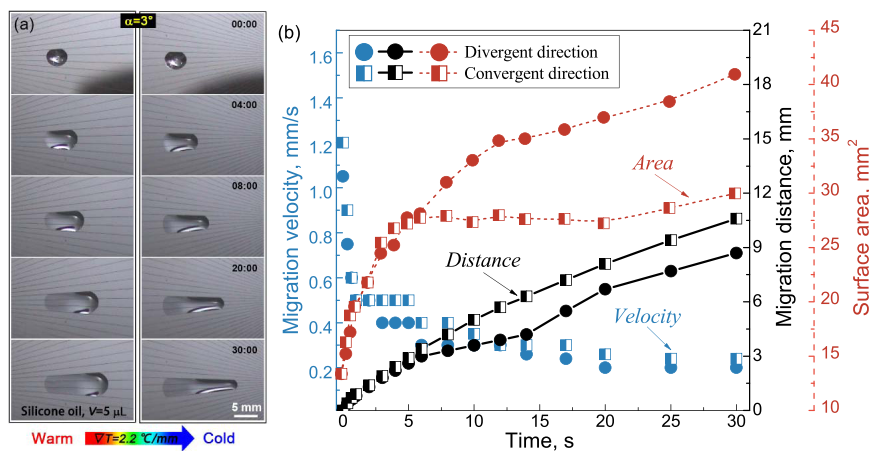


Figure 3. Results for the migration of a $5 \mu\text{L}$ silicone oil droplet on a radially grooved surface ($\alpha = 3^\circ$) in the convergent and divergent directions under a thermal gradient of $2.2^\circ\text{C}/\text{mm}$: (a) details of the migration process; (b) migration velocity, distance, and surface area of the liquid droplet vs the elapsed time.

simplify the fluid mechanical analysis,^{35–38} and it is relatively easy to identify the force balance acting on the liquid film.

Figure 5 shows a schematic of a migrating droplet on a radially microgrooved surface. According to the actual

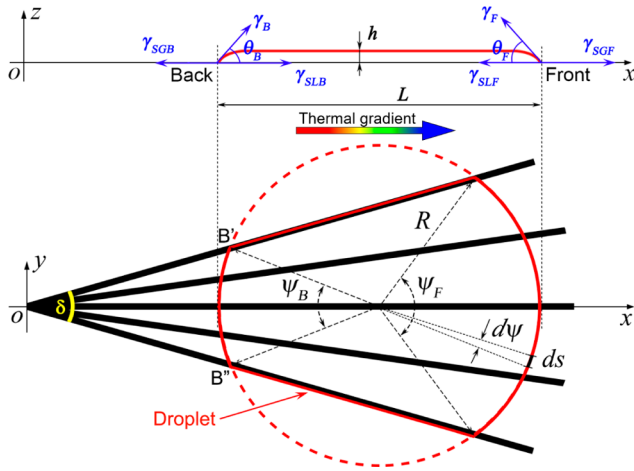


Figure 5. Ideal side and plan sketches of a migrating droplet on a radially microgrooved surface.

migration phenomenon shown in Figure 3a, the radial microgroove pattern leads to an asymmetric geometric morphology of the droplet at the front and back edges. Comparing and analyzing the extracted key frames from the videos reveals that a circle with a specified radius can basically cover the arc lengths at the front and back edges. Therefore, the footprint of the droplet is assumed to be a circle with a radius of R and different arc lengths at the front and back edges. The corresponding central angles are ψ_F and ψ_B ; X_F and X_B represent the front and back positions, respectively; h , L , and R represent the height, width, and radius of the droplet, respectively; γ (or γ_{LG}), γ_{SG} , and γ_{SL} represent the liquid–gas, solid–gas, and solid–liquid interfacial tensions, respectively.

Although the cross-sectional shape of the droplet varies with time (because the arc lengths at the front or back edges can increase in the divergent direction or decrease in the convergent direction as the migration progresses), at each time step, the migration can be regarded as a quasisteady process.³⁹ With these assumptions, the driving and resistance forces acting on the droplet per unit length along the x -direction were deduced.

Thermal Gradient-Induced Driving Force, F_T . For a droplet placed on a solid surface, Young's equation defines the interfacial tension force balance in the vicinity of the three-phase contact line⁴⁰

$$\gamma = \gamma_{SL} + \gamma_{LG} \cos \theta \quad (2)$$

The thermal gradient (C_T) is constant on the solid surface, i.e., $C_T = \frac{\partial T}{\partial x} = \text{const}$, and it is assumed that the temperature field within the droplet is exactly the same as that of the solid. When a constant thermal gradient is encountered, as indicated by the side view shown in Figure 5, variations in the interfacial tension at the solid–liquid surface are generated, i.e., the solid–gas interfacial tension (γ_F) at the front of the droplet is larger than that at the back (γ_B), and the force balance between the front and back edges is broken. This unbalanced force results in a traction vector that causes the droplet to migrate from a warm region toward a colder region.

This thermal gradient-induced driving force actually acts along the footprint of the droplet. As shown in the plan view in Figure 5, the x -component of the interfacial tension (γ) for an element length (ds) along the contact line of the droplet can be expressed as follows

$$df_{ix} = \gamma \cos \theta \cos \psi ds = \gamma R \cos \theta \cos \psi d\psi \quad (3)$$

where θ represents the contact angle and ψ represents the angle of the line connecting ds with the center of a circle relative to the x -axis.

Then, the interfacial force (f) resulting from the x -components of the interfacial tension, γ , acting on the droplet at the edges can be estimated as follows

$$f_x = \int_{-\psi_x/2}^{\psi_x/2} df_{ix} = \int_{-\psi_x/2}^{\psi_x/2} \gamma_x \cos \theta_x R \cos \psi d\psi \quad (4)$$

Because the interfacial tension increases with the decreasing temperature, the driving force generated along the footprint per unit length can be expressed as follows

$$F_T = \frac{1}{L} (f_{\text{Front}} - f_{\text{Back}}) \quad (5)$$

By combining eqs 1, 4, and 5, the driving force exerted on the droplet can be given as

$$F_T = 2R \cos \theta \left[(\gamma_0 + C_T \gamma_T x_F) \sin \frac{\psi_F}{2} - (\gamma_0 + C_T \gamma_T x_B) \sin \frac{\psi_B}{2} \right] \quad (6)$$

As shown in Figure 5, ψ depends on the corresponding arc length.

In this study, the initial divergence angles (α) all had a small order of magnitude. It is reasonable to assume that the arc length of $B'B''$ equals the linear length of $B'B''$; thus, the following equation is obtained

$$\psi_x = \frac{2x}{R} \tan \left(\frac{\delta}{2} \right) \quad (7)$$

where $\delta = N\alpha$, with N being the number of grooves covered by the liquid droplet; its values are 6 and 3 under divergence angles of 1 and 3°, respectively.

Viscous Resistance Force, F_V . The viscous resistance force generated during the migration can be calculated by integrating the viscous stress (σ_{xz}) over the base of the droplet, as follows

$$F_V = \int_{x_B}^{x_F} \sigma_{xz}(z=0) dx \quad (8)$$

Classically, the migration velocity is relatively slow; this motion conforms closely to the lubrication approximation limit. Therefore, the migration velocity profile, $V_x(z)$, of the droplet is governed by the simplified Navier–Stokes equation

$$\frac{\partial P}{\partial x} = \mu(x) \frac{\partial^2 V_x}{\partial z^2} \quad (9)$$

where P represents the pressure on the droplet and $\mu(x)$ represents the dynamic viscosity at location x .

Assuming that the substrate moves along the negative x -direction with a constant speed (U) so that the droplet remains stationary, the boundary conditions are as follows

$$\begin{cases} \frac{\partial V_x}{\partial z} = \frac{1}{\mu(x)} \frac{\partial \gamma}{\partial x}, z = h(x) \\ V_x = -U, z = 0 \end{cases} \quad (10)$$

By integrating eq 9 and applying the boundary conditions, the velocity field can be derived as follows

$$V_x(z) = \frac{1}{\mu(x)} \left[C_T \gamma_T z + \frac{1}{2} \frac{\partial P}{\partial x} (z^2 - 2zh) \right] - U \quad (11)$$

where C_T represents the thermal gradient on the solid surface.

In the moving frame of reference, the total volumetric flux across a section of the droplet at a specific x is zero; therefore,

$$\int_0^h V_x(z) dz = 0 \quad (12)$$

Substituting the velocity field equation (eq 11) into this constraint yields the pressure gradient. Then, the viscous stress (σ_{xz}) exerted by the solid surface on the liquid can be expressed as follows

$$\sigma_{xz(z=0)} = \mu(x) \left(\frac{\partial V_x}{\partial z} \Big|_{z=0} \right) = \frac{3\mu(x)}{h} U - \frac{1}{2} C_T \gamma_T \quad (13)$$

The viscosity of the liquid varies with respect to the temperature, and this variation can be approximated as follows

$$\mu(T) = \mu_0 e^{b(T-T_0)} \quad (14)$$

where μ_0 and $\mu(T)$ represent the viscosities at the reference temperature, T_0 , and at temperature T , respectively, and b is the viscosity–temperature coefficient.

Considering the thermal gradient on the solid surface, the viscosity, $\mu(x)$, can be rewritten as follows

$$\mu(x) = \mu_0 e^{b(T_C - C_T x - T_0)} \quad (15)$$

where T_C is the temperature at the initial position (center of the substrate).

By combining eqs 8, 13, and 15, and ignoring the curved parts at the rim, an exact analytical solution for the viscous resistance force (F_V) acting on the droplet can be obtained

$$F_V = \Phi(x_B, x_F) \frac{3\mu_0}{h} U - \frac{1}{2} \gamma_T C_T L \quad (16)$$

where

$$\Phi(x_B, x_F) = \frac{1}{bC_T} (e^{b(C_T x_B - T_C + T_0)} - e^{b(C_T x_F - T_C + T_0)}) \quad (17)$$

Capillary Force, F_C . As the migration progresses, the three-phase contact line moves forward, resulting in a variation in the free surface energy (E) of the solid–liquid–gas system, which can be expressed as follows⁴¹

$$\Delta E = (\gamma_{SL} - \gamma_{SG}) \Delta A_{SL} + \gamma_{LG} \Delta A_{LG} \quad (18)$$

where ΔA_{SL} and ΔA_{LG} represent the changing surface areas of the solid–liquid and liquid–gas interfaces, respectively.

By substituting Young's equation (eq 2) into eq 18, the variation in the free surface energy can be expressed as follows

$$\Delta E = \gamma_{LG} (\Delta A_{LG} - \Delta A_{SL} \cos \theta) \quad (19)$$

The capillary forces act on both sides of the droplet. Compared with the thermal gradient-induced surface-tension force, the capillary force in the direction opposing the thermal gradient is

far smaller; thus, we ignore it. Because the contact angle of the silicone oil on the silicon surface is small (only approximately 10° ; see Figure 1), it is reasonable to assume that the silicone oil droplet can easily spread into the grooves. Then, the capillary force can be deduced from the gradient of the total free surface energy. Following the simplification proposed by Rye,⁴² this force acting on the droplet per unit length can be given as

$$F_C = \frac{N}{L} \gamma_{LG} [(w + 2h_0) \cos \theta - w] \quad (20)$$

where w and h_0 represent the width and depth of the groove, respectively, as shown in Table 2.

Steady-State Equation. As the droplet moves steadily on the radially microgrooved surface, the driving forces are assumed to be equal to the resistance forces. In both the convergent and the divergent directions, the microgroove-induced capillary force always influences the migration behavior. The steady-state equation for the motion can be established as follows

$$F_V = F_T + F_C \quad (21)$$

Finally, substituting eqs 6, 16, and 20 into eq 21 yields the theoretical expression for the migration velocity on a radially microgrooved surface

$$U = \frac{h}{3\mu_0 L \Phi(x_B, x_F)} \left\{ \frac{1}{2} \gamma_T C_T L^2 + 2R \cos \theta \left(\gamma_F \sin \frac{\psi_F}{2} - \gamma_B \sin \frac{\psi_B}{2} \right) + N\gamma[(w + 2h_0) \cos \theta - w] \right\} \quad (22)$$

Validation. Figure 6 shows the experimental and numerical results for a droplet migrating on a radially microgrooved

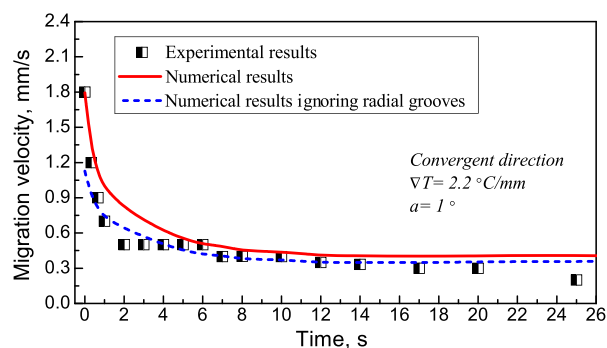


Figure 6. Experimental and numerical results for a droplet migrating on a radially microgrooved surface ($\alpha = 1^\circ$) in the convergent direction.

surface ($\alpha = 1^\circ$) in the convergent direction subject to a thermal gradient of $2.2^\circ\text{C}/\text{mm}$. As indicated by the line graph, initially, the numerical migration velocity was approximately 1.8 mm/s ; it decreased rapidly within 5 s and then gradually over time. The numerical results agree well with the experimental data (scatter points). Meanwhile, when the capillary force induced by the radial microgrooves is ignored, the numerical results consistently have a lower amplitude than the experimental results, as indicated by the dotted line. This confirms that the radial microgroove-induced capillary force

can contribute to the migration, which makes the results more reasonable.

To further validate the derivation, the migration velocities on radially microgrooved surfaces with different divergence angles (α) in the convergent and divergent directions were calculated, as shown in Figure 7. With $\alpha = 1^\circ$, as shown in

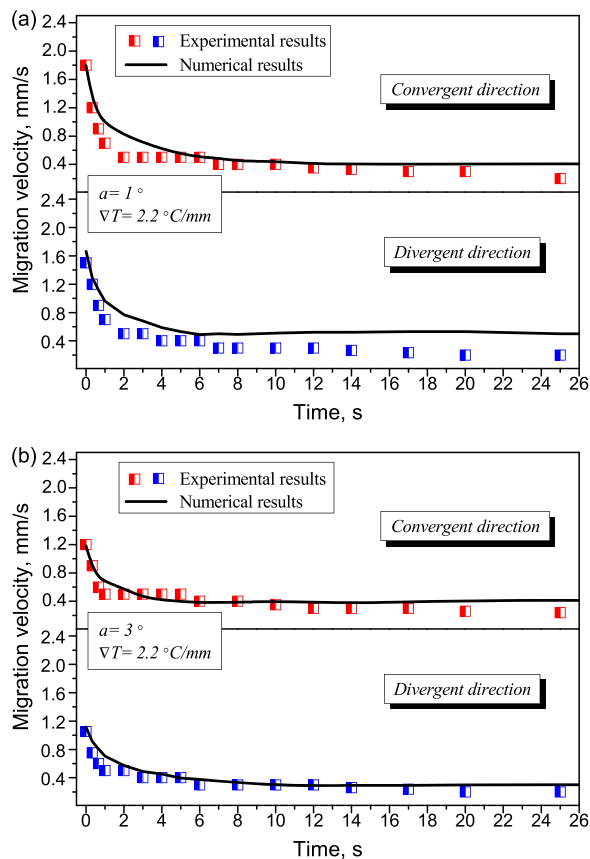


Figure 7. Experimental and numerical results for a droplet migrating on a radially microgrooved surface in the convergent and divergent directions.

Figure 7a, the initial experimental migration velocities in the convergent and divergent directions were 1.79 and 1.5 mm/s, respectively, and the corresponding numerical results were 1.8 and 1.65 mm/s, respectively. Note that the numerical results are in good agreement with the experimental data, despite the existence of a slight difference as the migration progressed. With $\alpha = 3^\circ$, as shown in Figure 7b, the larger initial divergence angle yielded a lower migration velocity. Generally, a smaller divergence angle results in a smaller spreading area and therefore leads to a higher migration velocity, in addition to a larger number of wetted grooves. Moreover, when the surface includes radial microgrooves, a capillary force is generated. Whether the migration occurs in the convergent or divergent direction, this force always exists and contributes to the movement. It can be inferred that a larger number of grooves yields a larger capillary force. For a droplet with a constant volume ($5 \mu\text{L}$), a microgrooved surface with a smaller divergence angle has a larger number of grooves wetted by the droplet. According to eq 20, the theoretical expression for the capillary force is proportional to the number of grooves covered by the liquid droplet. Therefore, a surface with a smaller divergence angle has a higher migration velocity.

Overall, for both the convergent and divergent directions, the predicted results were always in accordance with the experimental results; they were both initially high and decreased gradually over time. These comprehensive comparisons validate the theoretical derivation.

Further Discussion. In this study, we investigated the droplet migration on radially microgrooved surfaces experimentally and theoretically. The dominant forces acting on the droplet were identified: the thermal gradient-induced Young's force and microgroove-induced capillary force are balanced by the viscous resistance force generated within the liquid during the migration. The initial migration process is complicated, as when a droplet is placed on a surface subjected to a thermal gradient, wetting and migration processes occur simultaneously. This means that the initial high migration velocity has contributions from the wetting and migration velocities, for which the acceleration and deceleration change in the first few seconds with the disappearing of the initial wetting effect, resulting in a rapid decrease in the migration velocity.

Note that the radial grooves yield a deformation of the droplet shape during the migration process, which changes the interfacial forces at the front and back edges. Therefore, we considered this deformation effect and substituted a position-dependent arc length into the theoretical derivation; moreover, the radial grooves alter the spreading area of the droplet. The derived theoretical migration velocity (eq 22) reveals the existence of a positive correlation between the migration velocity and the thickness of the spreading droplet. This indicates that a thicker droplet film can yield a higher migration velocity. As indicated by the experimental results in Figure 3, the spreading area of a droplet in the convergent direction is smaller than that in the divergent direction. Therefore, under the same experimental conditions, the convergent direction yields a higher migration velocity than the divergent direction.

The proposed theoretical model agrees well with the experimental data obtained under different experimental conditions. Nevertheless, slight differences exist owing to several assumptions and simplifications. First, considering the microgroove-induced capillary force while ignoring the viscosity resistance introduces an error. Rye⁴² presented an approach to quantify this resistance force; while it involves more assumptions and parameters that are difficult to measure, more accurate predictions can be obtained at the cost of additional theoretical derivations and experimental measurements. Second, as the droplet migrates forward, some liquid remains along the trajectory and in the grooves; neglecting this residual oil can also introduce an error. Furthermore, the temperature of the droplet is not equal to that of the solid surface on which it is placed, and considering the efficiency of the heat conduction between the solid and liquid would increase the accuracy of the results.

CONCLUSIONS

Numerous studies have indicated that intelligently designed microgrooves with disparate topographies with regard to their shape, geometry, density, or arrangement mode have idiosyncratic effects on the thermocapillary migration of liquid droplets. However, the divergent direction and initial divergence angle are also important parameters, and there have been few investigations of these aspects. Hence, we performed an experimental and theoretical investigation of thermocapillary migration on radially microgrooved surfaces.

Migration experiments with silicone oil droplets were performed on radially microgrooved surfaces, and the effects of the divergent direction and initial divergence angle on the migration performance were examined. Previous studies have revealed that the migration velocity on smooth surfaces can be predicted by balancing the thermal gradient-induced driving force with the viscous resistance force. Thus, we established a theoretical model by taking the thermocapillary, viscous resistance, and radial structure-induced forces into account. Relative to the experimental results, the proposed theoretical expression exhibited a high accuracy. This study advances the understanding of interfacial phenomena and provides general guidance for the design of radial microgroove patterns, which have great prospects for regulating and controlling the liquid motion in lubrication systems, condensation and heat-transfer devices, and open microfluidics.

AUTHOR INFORMATION

Corresponding Author

*E-mail: daiqingwen@nuaa.edu.cn.

ORCID

Qingwen Dai: 0000-0001-7422-4259

Notes

The authors declare no competing financial interest.

ACKNOWLEDGMENTS

The authors are grateful for the support provided by the National Nature Science Foundation of China (grant no. 51805252) and China Postdoctoral Science Foundation (grant no. 2019M651822) and National Key Laboratory of Science and Technology on Helicopter Transmission (Nanjing University of Aeronautics & Astronautics) (grant no. HTL-A-18G01).

REFERENCES

- (1) Tadmor, R. Marangoni flow revisited. *J. Colloid Interface Sci.* **2009**, *332*, 451–454.
- (2) Bonn, D.; Eggers, J.; Indekeu, J.; Meunier, J.; Rolley, E. Wetting and spreading. *Rev Mod Phys* **2009**, *81*, 739–805.
- (3) Tadmor, R. Approaches in wetting phenomena. *Soft Matter* **2011**, *7*, 1577–1580.
- (4) Dai, Q.; Huang, W.; Wang, X. Surface roughness and orientation effects on the thermo-capillary migration of a droplet of paraffin oil. *Exp. Therm. Fluid Sci.* **2014**, *57*, 200–206.
- (5) Bormashenko, E.; Bormashenko, Y.; Gryniov, R.; Aharoni, H.; Whyman, G.; Binks, B. P. Self-propulsion of liquid marbles: Leidenfrost-like levitation driven by marangoni flow. *J. Phys. Chem. C* **2015**, *119*, 9910–9915.
- (6) Daniel, S.; Chaudhury, M. K.; Chen, J. C. Fast drop movements resulting from the phase change on a gradient surface. *Science* **2001**, *291*, 633–636.
- (7) Karapetsas, G.; Sahu, K. C.; Sefiane, K.; Matar, O. K. Thermocapillary-driven motion of a sessile drop: Effect of non-monotonic dependence of surface tension on temperature. *Langmuir* **2014**, *30*, 4310–4321.
- (8) Dai, Q.; Khonsari, M. M.; Shen, C.; Huang, W.; Wang, X. Thermocapillary migration of liquid droplets induced by a unidirectional thermal gradient. *Langmuir* **2016**, *32*, 7485–7492.
- (9) Karapetsas, G.; Chamakos, N. T.; Papatheanasiou, A. G. Thermocapillary droplet actuation: Effect of solid structure and wettability. *Langmuir* **2017**, *33*, 10838–10850.
- (10) Ryazantsev, Y. S.; Velarde, M. G.; Guzman, E.; Rubio, R. G.; Ortega, F.; Montoya, J.-J. On the autonomous motion of active drops or bubbles. *J. Colloid Interface Sci.* **2018**, *527*, 180–186.
- (11) Liu, J.; Li, S. Capillarity-driven migration of small objects: A critical review. *Eur. Phys. J. E* **2019**, *42*, No. 1.
- (12) Sommers, A. D.; Jacobi, A. M. Wetting phenomena on microgrooved aluminum surfaces and modeling of the critical droplet size. *J. Colloid Interface Sci.* **2008**, *328*, 402–411.
- (13) Jones, W. R.; Jansen, M. J. Tribology for space applications. *Proc. Inst. Mech. Eng., Part J* **2008**, *222*, 997–1004.
- (14) Chaudhury, M. K.; Chakrabarti, A.; Daniel, S. Generation of motion of drops with interfacial contact. *Langmuir* **2015**, *31*, 9266–9281.
- (15) Bakli, C.; P, D. S.; Chakraborty, S. Mimicking wettability alterations using temperature gradients for water nanodroplets. *Nanoscale* **2017**, *9*, 12509–12515.
- (16) Bormashenko, E.; Frenkel, M.; Bormashenko, Y.; Chaniel, G.; Valtsifer, V.; Binks, B. P. Superposition of translational and rotational motions under self-propulsion of liquid marbles filled with aqueous solutions of camphor. *Langmuir* **2017**, *33*, 13234–13241.
- (17) Roberts, E. W.; Todd, M. J. Space and vacuum tribology. *Wear* **1990**, *136*, 157–167.
- (18) Rahman, M. A.; Jacobi, A. M. Wetting behavior and drainage of water droplets on microgrooved brass surfaces. *Langmuir* **2012**, *28*, 13441–13451.
- (19) Wu, J.; Ma, R. Y.; Wang, Z. K.; Yao, S. H. Do droplets always move following the wettability gradient? *Appl. Phys. Lett.* **2011**, *98*, No. 2014104.
- (20) Yu, H.; Huang, W.; Wang, X. Dimple patterns design for different circumstances. *Lubr. Sci.* **2013**, *25*, 67–78.
- (21) Li, J.; Hou, Y.; Liu, Y.; Hao, C.; Li, M.; Chaudhury, M. K.; Yao, S.; Wang, Z. Directional transport of high-temperature janus droplets mediated by structural topography. *Nat. Phys.* **2016**, *12*, 606–612.
- (22) Zhang, P.; Chen, H.; Li, L.; Liu, H.; Liu, G.; Zhang, L.; Zhang, D.; Jiang, L. Bioinspired smart peristome surface for temperature-controlled unidirectional water spreading. *ACS Appl. Mater. Interfaces* **2017**, *9*, 5645–5652.
- (23) Herminghaus, S.; Brinkmann, M.; Seemann, R. Wetting and dewetting of complex surface geometries. *Annu. Rev. Mater. Res.* **2008**, *38*, 101–121.
- (24) Grützmacher, P. G.; Rosenkranz, A.; Gachot, C. How to guide lubricants-tailored laser surface patterns on stainless steel. *Appl. Surf. Sci.* **2016**, *370*, 59–66.
- (25) Dai, Q.; Huang, W.; Wang, X. Micro-grooves design to modify the thermo-capillary migration of paraffin oil. *Meccanica* **2017**, *52*, 171–181.
- (26) Sommers, A. D.; Brest, T. J.; Eid, K. F. Topography-based surface tension gradients to facilitate water droplet movement on laser-etched copper substrates. *Langmuir* **2013**, *29*, 12043–12050.
- (27) Grützmacher, P. G.; Rosenkranz, A.; Szurdak, A.; Gachot, C.; Hirt, G.; Mücklich, F. Lubricant migration on stainless steel induced by bio-inspired multi-scale surface patterns. *Mater. Des.* **2018**, *150*, 55–63.
- (28) Bliznyuk, O.; Jansen, H. P.; Kooij, E. S.; Zandvliet, H. J.; Poelsema, B. Smart design of stripe-patterned gradient surfaces to control droplet motion. *Langmuir* **2011**, *27*, 11238–11245.
- (29) Zheng, Y.; Cheng, J.; Zhou, C.; Xing, H.; Wen, X.; Pi, P.; Xu, S. Droplet motion on a shape gradient surface. *Langmuir* **2017**, *33*, 4172–4177.
- (30) Dai, Q.; Huang, W.; Wang, X. A surface texture design to obstruct the liquid migration induced by omnidirectional thermal gradients. *Langmuir* **2015**, *31*, 10154–10160.
- (31) Li, M.; Huang, W.; Wang, X. Bioinspired, peg-studded hexagonal patterns for wetting and friction. *Biointerphases* **2015**, *10*, No. 031008.
- (32) Brochard, F. Motions of droplets on solid surfaces induced by chemical or thermal gradients. *Langmuir* **1989**, *5*, 432–438.
- (33) Dai, Q.; Huang, W.; Wang, X.; Khonsari, M. M. Ringlike migration of a droplet propelled by an omnidirectional thermal gradient. *Langmuir* **2018**, *34*, 3806–3812.

- (34) Dai, Q.; Huang, W.; Wang, X. Contact angle hysteresis effect on the thermocapillary migration of liquid droplets. *J. Colloid Interface Sci.* **2018**, *515*, 32–38.
- (35) Mettu, S.; Chaudhury, M. K. Motion of drops on a surface induced by thermal gradient and vibration. *Langmuir* **2008**, *24*, 10833–10837.
- (36) Chaudhury, K.; Chakraborty, S. Spreading of a droplet over a nonisothermal substrate: Multiple scaling regimes. *Langmuir* **2015**, *31*, 4169–4175.
- (37) Brzoska, J. B.; Brochard-Wyart, F.; Rondelez, F. Motions of droplets on hydrophobic model surfaces induced by thermal gradients. *Langmuir* **1993**, *9*, 2220–2224.
- (38) Ford, M. L.; Nadim, A. Thermocapillary migration of an attached drop on a solid surface. *Phys. Fluids* **1994**, *6*, 3183–3185.
- (39) Pratap, V.; Moumen, N.; Subramanian, R. S. Thermocapillary motion of a liquid drop on a horizontal solid surface. *Langmuir* **2008**, *24*, 5185–5193.
- (40) Tadmor, R. Line energy and the relation between advancing, receding, and young contact angles. *Langmuir* **2004**, *20*, 7659–7664.
- (41) Good, R. J. The rate of penetration of a fluid into a porous body initially devoid of adsorbed material (1, 2). *J. Colloid Interface Sci.* **1973**, *42*, 473–477.
- (42) Rye, R. R.; Yost, F. G.; O'Toole, E. J. Capillary flow in irregular surface grooves. *Langmuir* **1998**, *14*, 3937–3943.